Flow and heat transfer characteristics of a Dusty UCM fluid over a permeable stretching surface

HANUMESH VAIDYA
Department of Mathematics, SSA Government First Grade College (Autonomous),
Ballari-583 101, Karnataka, India.
Email: hanumeshvaidya@gmail.com

Abstract: This article examines the characteristics of flow and heat transfer of a dusty UCM fluid over a permeable elastic sheet. The flow is induced due to an infinite elastic sheet which is stretched in its own plane. Using a similarity transformation, the governing non-linear partial differential equations of the model problem are transformed into coupled non-linear ordinary differential equations and these equations are solved numerically by a second-order finite difference implicit method. The effects of the physical parameters on the fluid velocity, the velocity of the dust particle, the density of the dust particle, the fluid temperature, the dust-phase temperature, the skin friction, and the wall-temperature gradient are assessed through tables and graphs. One of the important observations is that Maxwell fluid reduces the wall-shear stress. The results obtained for the flow characteristics reveal many interesting behaviors that warrant further study on the non-Newtonian fluid phenomena, especially the dusty UCM fluid phenomena.

Keywords: Stretching sheet, Dusty fluid, Fluid particle interaction parameter, Finite difference method.

1. Introduction

In recent years flow through porous sheet has gained a momentum due to its industrial application such as metallurgical processes involve the cooling of continuous strips or filaments by drawing them through a quiescent fluid. The rate of cooling can be controlled and final product of desired characteristics can be achieved if strips are drawn through porous media. In view of this, the study of visco-elastic fluid flow through porous media has gained importance in recent years; the heat transfer due to a continuously moving surface through an ambient liquid is one of the important thrust areas of current research due to their extensive applications arises in a broad spectrum of science and engineering disciplines. Sakiadis [1] was the first among the others to study the boundary layer flow generated by a continuous solid surface moving with constant velocity. Crane [2] continued the work of Sakiadis [1] to a polymer industry to study a steady two-dimensional boundary layer flow caused by stretching of a sheet that moves in its plane with a velocity which varies linearly with the distance from a fixed point on the sheet. Many investigators have extended the work of Crane to study heat and mass transfer under different physical situations (Grubka and Bobba [3], Datta et al [4], Chen and Char [5], Ali [6], Ishak et al [7], Prasad et al [8-12]). In these works, the fluid was assumed to be Newtonian or considered Newtonian fluid as a base fluid. However, many industrial fluids are non-Newtonian in nature or rheological in their flow characteristics such as molten plastics, polymers, suspension, foods, slurries, paints, glues, printing inks, blood. That is, they might exhibit dynamic deviation from Newtonian behavior depending upon the flow configuration and/or the rate of deformation. These fluids often obey non-linear constitutive equations and the complexity of these constitutive equations is the main culprit for the lack of exact analytical solutions. For example, visco-elastic fluid models considered in these works are simple models, such as second order fluid model and Walters' model (Rajagopal et al. [13], Char [14]), which are known to be good for weakly elastic fluids subjected to slowly varying flows. These two models are known to violate certain rules of thermodynamics. Therefore significance of the results reported in the above works is limited as far as the polymer industry is concerned. Obviously for the theoretical results to become of any industrial importance, more general visco-elastic fluid

models such as upper convected Maxwell model or Oldroyd B model should be invoked in the analysis. Indeed these two fluid models are being used recently to study the visco-elastic fluid flow over a stretching and non-stretching sheets with or without heat transfer (Bhatnagar et al. [15], Sadeghy et al [16], Vajravelu et al [17])).

All the above investigators restrict their analyses to the flow induced by a stretching sheet in the absence of fluid-particle suspension. The analysis of two-phase flows in which solid spherical particles are distributed in a fluid is of interest in a wide range of technical problems such as flow through packed beds, sedimentation, environmental pollution, centrifugal separation of particles and blood rheology. The study of the boundary layer of fluid-particle suspension flow is important in determining the particle accumulation and impingement of the particle on the surface. Saffman [18] investigated the stability of the laminar flow of a dusty gas in which the dust particles are uniformly distributed. Datta and Mishra [19] explore the dusty fluid in boundary layer flow over a semi-infinite flat plate. In these studies, the physical properties of the ambient fluid were assumed to be constant. However, it is known that these physical properties of the ambient fluid may change with temperature. For lubricating fluids, heat generated by internal friction and the corresponding rise in the temperature affects the thermal conductivity of the fluid so it can no longer be assumed constant. The increase of temperature leads to increase in the transport phenomena by reducing the thermal conductivity across the thermal boundary layer due to which the heat transfer at the wall is also affected. Therefore to predict the flow and heat transfer rates, it is necessary to take variable thermal conductivity of the fluid into account. Available literature on variable thermal conductivity and fluid-particle interaction shows that combined work has not been carried out for UCM fluid over a stretching sheet.

Motivated by these analysis, in the present paper, the authors envisage to study the flow and heat transfer of a dusty non-Newtonian UCM fluid over a porous stretching sheet. Because of the non-Newtonian rheology, the fluid-particle interaction, the momentum and energy equations for both the fluid as well as dust phase are highly non-linear, and coupled form of partial differential equations (PDEs). These PDEs are then converted to couple, non-linear ordinary differential equations (ODEs) by using the similarity variables along with the appropriate boundary conditions. Because of the complexity and the non-linearly in the problem, we propose to solve these equations by a second order finite difference scheme by Keller box method (Vejravelu and Prasad [20]). The effect of pertinent parameters on the velocity and temperature fields, the skin friction coefficient and the local Nusselt number for both cases are presented in graphically and few of them are recorded in Tables. It is believed that the results obtained from the present investigation will provide useful information for applications and will also serve as a complement to previous studies.

2. Mathematical Formulation

Consider a steady two-dimensional, boundary layer flow of a viscous, incompressible, dusty non-Newtonian fluid, namely, UCM fluid over a horizontal stretching sheet with a stretching velocity $U_w(x) = bx$, and prescribed surface temperature $T_w(x) = A(x/l)$; where $b > 0$ is the stretching velocity rate, l is the reference length scale and A is the constant. The sheet is coinciding with the plane $y = 0$, with the flow being confined to $y > 0$. Two equal and opposite forces are introduced along the x-axis, so that the sheet is stretched, the origin is fixed (see Fig. 1). The thermo-physical fluid properties are assumed to be isotropic and constant, except for the thermal conductivity which is assumed to vary as a function of temperature in the following form

$$K(T) = K_\infty \left(1 + \frac{\varepsilon}{\Delta T}(T - T_\infty)\right), \qquad (1)$$

where $K(T)$ is the temperature dependent fluid thermal conductivity, K_∞ is the thermal conductivity far away from the slit respectively, $\varepsilon = (K_w - K_\infty)/K_\infty$ is a small parameter known as variable thermal conductivity parameter, K_w is the thermal conductivity at the surface and $\Delta T = T_w - T_\infty$, T_w is the surface temperature and T_∞ is the ambient temperature. Further, the flow region is exposed under the influence of permeability of the porous medium. The viscous dissipation and the ohmic heating terms are not included in

the energy equation since they are, generally small. Here, the fluid and the dust particle clouds are suppose to be static at the beginning. The dust particles are assumed to be spherical in shape and uniform in size and number density of the dust particle is taken as a constant throughout the flow. Under these conditions, the basic boundary-layer equations for continuity, conservation of mass (with no pressure gradient), and energy for clear UCM fluid as well as dusty fluid can be written as

$$\frac{\partial u}{\partial x}+\frac{\partial \mathrm{v}}{\partial y}=0, \tag{2}$$

$$u\frac{\partial u}{\partial x}+\mathrm{v}\frac{\partial u}{\partial y}+\lambda\left(u^2\frac{\partial^2 u}{\partial x^2}+\mathrm{v}^2\frac{\partial^2 u}{\partial y^2}+2u\mathrm{v}\frac{\partial^2 u}{\partial x\partial y}\right)=\nu\frac{\partial^2 u}{\partial y^2}-\frac{\nu}{K'}u-\frac{\rho_p}{\rho\tau}\left(u-u_p\right), \tag{3}$$

$$u_p\frac{\partial u_p}{\partial x}+\mathrm{v}_p\frac{\partial u_p}{\partial y}=\frac{1}{\tau}\left(u-u_p\right), \tag{4}$$

$$u_p\frac{\partial \mathrm{v}_p}{\partial x}+\mathrm{v}_p\frac{\partial \mathrm{v}_p}{\partial y}=\frac{1}{\tau}\left(\mathrm{v}-\mathrm{v}_p\right), \tag{5}$$

$$\frac{\partial}{\partial x}\left(\rho_p u_p\right)+\frac{\partial}{\partial y}\left(\rho_p \mathrm{v}_p\right)=0, \tag{6}$$

$$u\frac{\partial T}{\partial x}+\mathrm{v}\frac{\partial T}{\partial y}=\frac{\partial}{\partial y}\left(\frac{K(T)}{\rho c_p}\frac{\partial T}{\partial y}\right)+\frac{\rho_p c_s}{\rho\gamma_T c_p}\left(T_P-T\right), \tag{7}$$

$$u_p\frac{\partial T_p}{\partial x}+\mathrm{v}_p\frac{\partial T_p}{\partial y}=-\frac{1}{\gamma_T}\left(T_P-T\right). \tag{8}$$

where (u,v) and (u_p,v_p) are the velocities components of the fluid and dust particle phases along the x and y axes, respectively, ρ is the density of the fluid. Here $\tau=1/k$ is the relaxation time of particles, k is the Stokes' constant $(=6\pi\mu D)$, μ is the coefficient of viscosity and D is the average radius of the dust particles. Further, K' is the permeability of the porous medium, λ is the relaxation time and ρ_p is the mass of the dust particles per unit volume of the fluid. $K(T)$ is the temperature dependent thermal conductivity, T and T_p are respectively, the temperatures of the fluid and the dust phase particles. Further, c_p and c_s are, respectively, the specific heat capacity of the fluid and specific heat capacity of the dust particles, γ_T is the temperature relaxation time $\left(=3\ \mathrm{Pr}\ \gamma_p c_p/2c_p\right)$; γ_p is the velocity relaxation time $(=1/k)$; and Pr is the usual Prandtl number. It is assumed that the normal stress is of the same order of magnitude as that of the shear stress in addition to the usual boundary layer approximation for deriving the *x*-component of the momentum boundary layer equation (3). The last term in Eq. (3) represents the force due to the relative motion between the fluid and the dust particles. In such a case the force between the dust and the fluid is proportional to the relative velocity. In deriving these equations the Stokesian drag force is considered for the interaction between the fluid and the particle phases. The appropriate boundary conditions on velocity and temperature are

$$\begin{aligned}&u=U_w(x)=bx,\quad \mathrm{v}=0,\quad T=T_w=A\left(x/l\right)\quad at\quad y=0,\\&u\to 0,\ u_p\to 0,\ \mathrm{v}_p\to \mathrm{v},\ \rho_p\to k\rho, T\to T_\infty,\ T_p\to T_\infty\quad as\quad y\to\infty.\end{aligned} \tag{9}$$

To convert the governing equations into a set of similarity equations, we introduce the following transformation as mentioned below

$$\begin{aligned}&\eta=\sqrt{\frac{b}{\nu}}y,\ u=bx\,f'(\eta),\quad \mathrm{v}=-\sqrt{b\nu}\,f(\eta),\ u_p=bxF(\eta),\ \mathrm{v}_p=\sqrt{b\nu}G(\eta),\\&\rho_r=H(\eta),\ T-T_\infty=\left(T_w-T_\infty\right)\theta(\eta),\ T_P-T_\infty=\left(T_w-T_\infty\right)\theta_P(\eta),\quad T_w-T_\infty=A\left(x/l\right)\end{aligned} \tag{10}$$

here η is the similarity variable and prime denotes the differentiation with respect to η, $\rho_r = \rho_p/\rho$ is the relative density, $f, F, G, H, \theta, \theta_p$ are dimensionless quantities and ν is the kinematic viscosity. Substituting Eq. (10) into Eq. (3) - (8), we obtain the following coupled non-linear ordinary differential equation

$$\begin{aligned}
&f''' + f\,f'' - f'^2 + \beta_1\left(2f\,f'\,f'' - f^2 f'''\right)\\
&-K_1 f' + H\beta\left(F - f'\right) = 0,\\
&GF' + F^2 + \beta\left(F - f'\right) = 0,\\
&GG' + \beta\left(f + G\right) = 0\ ,\\
&GH' + HG' + FH = 0,
\end{aligned} \tag{11}$$

$$\left((1+\varepsilon\theta)\theta'\right)' - \Pr\begin{vmatrix} f' & \theta' \\ f & \theta \end{vmatrix} + \frac{2}{3}\beta H\left(\theta_P - \theta\right) = 0, \tag{12}$$

$$2F\theta_P + G\theta_P' + L_0\beta\left(\theta_P - \theta\right) = 0$$

subjected to the boundary conditions

$$\begin{aligned}
&f' = 1, \quad f = 0, \quad \theta = 1 \quad at\ \eta = 0,\\
&f' \to 0,\ F \to 0,\ G \to -f,\ H \to k,\ \theta \to 0,\ \theta_P \to 0\ as\ \eta \to \infty,
\end{aligned} \tag{13}$$

where $K_1 = \nu/K'b$ is the porosity parameter, $\beta = 1/b\tau$ is the fluid-particle interaction parameter, $\beta_1 = \lambda b$ is the Maxwell parameter, and $L_0 = \tau/\gamma_T$ is the temperature relaxation parameter. The physical quantities of interest are the skin friction coefficient C_f and the local Nusselt number Nu_x which are defined by

$$C_f = \frac{\tau_w}{\rho_\infty U_w^2/2},\ Nu_x = \frac{xq_w}{k_\infty\left(T_w - T_\infty\right)} \tag{14}$$

where τ_w is the surface shear stress and q_w the surface heat flux are given by

$$\tau_w = \mu_\infty\left(\frac{\partial u}{\partial y}\right)_{y=0},\ q_w = -K_\infty\left(\frac{\partial T}{\partial y}\right)_{y=0} \tag{15}$$

Using the similarity variables (10), we obtain

$$\frac{1}{2}C_f\,\mathrm{Re}_x^{1/2} = f''(0),\ \text{and}\ \frac{Nu_x}{\mathrm{Re}_x^{1/2}} = -\theta'(0) \tag{16}$$

where $\mathrm{Re}_x = U_w x/\nu$ is the local Reynolds number.

3. Numerical Procedure

The system of Eqs. (11) and (12) are coupled and highly nonlinear. Exact analytical solutions are not possible for the complete set of equations and, therefore, we use the efficient numerical method with second-order finite difference scheme known as the Keller–box method [20]. These coupled non-linear ordinary differential equations (11) and (12) (third order in $f(\eta)$, first order in $F(\eta)$, $G(\eta)$, $H(\eta)$, $\theta_p(\eta)$ and second order in $\theta(\eta)$, respectively) are reduced to a system of nine simultaneous ordinary differential equations of first order with nine unknowns, by assuming $f = f_1$, $f' = f_2$, $f'' = f_3$, $\theta = \theta_1$, $\theta' = \theta_2$. To solve this system of equations we require nine initial conditions while we have only two initial conditions $f(0)$, $f'(0)$ on $f(\eta)$ and one initial condition $\theta(0)$ on $\theta(\eta)$. The other six initial conditions $f''(0)$, $F(0)$, $G(0)$, $H(0)$, $\theta'(0)$ and $\theta_p(0)$ are not known. However, the values of $f'(\eta)$, $F(\eta)$, $G(\eta)$, $H(\eta)$, $\theta(\eta)$ and $\theta_p(\eta)$ are known as $\eta \to \infty$. Now, we employ the Keller – Box scheme where these six boundary conditions are utilized to produce six unknown initial conditions at $\eta = 0$. To select η_∞, we begin with some initial guess values and solve the boundary value problem with some particular set of parameters to obtain $f''(0)$, $F(0)$, $G(0)$, $H(0)$, $\theta'(0)$ and $\theta_p(0)$. Thus, we start with

the initial approximations as $f''(0)=\delta_1, F(0)=\delta_2, G(0)=\delta_3, H(0)=\delta_4, \theta'(0)=\delta_5$ and $\theta_p(0) = \delta_6$. Let $\delta_i (i=1,2,3,4,5,6)$ be the correct values of $f''(0)$, $F(0)$, $G(0)$, $H(0)$, $\theta'(0)$ and $\theta_p(0)$. We integrate the resulting system of nine ordinary differential equations using the fourth-order Runge–Kutta method and obtain the values of $f''(0)$, $F(0)$, $G(0)$, $H(0)$, $\theta'(0)$ and $\theta_p(0)$. The solution process is repeated with another larger value of η_∞ until two successive values of $f''(0)$, $F(0)$, $G(0)$, $H(0)$, $\theta'(0)$ and $\theta_p(0)$ differ only after desired digit signifying the limit of the boundary along η. The last value of η_∞ is chosen as the appropriate value for that particular set of parameters. Finally, the problem can be solved numerically using a second-order finite difference scheme known as the Keller – Box method. The numerical solutions are obtained in four steps as follows:

- Reduce the systems of Eq. (11) and (12) to a system of first order equations.
- Write the difference equations using central differences.
- Linearize the algebraic equations by Newton's method, and write them in matrix-vector form.
- Solve the linear system by the block tri-diagonal elimination technique.

For the sake of brevity, the details of the numerical procedure are not presented here. It is also important to note that the computational time for each set of input parameters should be short. Because physical domain in this problem is unbounded, whereas the computational domain has to be finite, we apply the far field boundary conditions for the similarity variable η at finite value denoted by $\eta_{\max}$. We ran our bulk of computations with the value $\eta_{\max}=7$, which is sufficient to achieve the far field boundary conditions asymptotically for all values of the parameters considered. For numerical calculations, a uniform step size of $\Delta\eta = 0.01$ is found to be satisfactory and the solutions are obtained with an error tolerance of 10^{-6} in all the cases. The accuracy of the numerical scheme is validated by comparing the skin friction and the rate of heat transfer results with those available in the literature. These results agree very well (see Table 1).

4. Discussion of the Results

In this section, we illustrate the effects of the pertinent parameters, namely, the fluid-particle interaction parameter β, the Maxwell parameter β_1, the Porous parameter K_1, the variable thermal conductivity parameter ε, and the Prandtl number $\Pr$ on the flow and heat transfer of non-Newtonian UCM fluid over a horizontal stretching sheet. The temperature relaxation parameter L_0 is chosen as unity throughout the computation. The numerical solution for the most general case is obtained by using a second-order implicit finite difference scheme known as the Keller–Box method. In order to analyze the salient features of the problem, the numerical results are illustrated graphically in Figs 1-5. Also the numerical illustration of the results for the skin friction, the particle velocity and the density components, the fluid temperature, and the dust-phase temperature at the surface for different values of the physical parameters are recorded in Table 2.

The transverse velocity $f(\eta)$, the horizontal velocity $f'(\eta)$, the particle transverse velocity $F(\eta)$ and the particle horizontal velocity $G(\eta)$ profiles are shown graphically in Figs. 1(a)–1(d) for different values of K_1 and β. The general trend is that $f'(\eta)$, $F(\eta)$ and $G(\eta)$ decrease monotonically as the distance increases from the surface, whereas $f(\eta)$ increases as the distance increases from stretching sheet. It is observed from these figures that $f'(\eta)$ and $F(\eta)$ profiles decrease with an increase in K_1. This observation holds true even with particle velocity component $F(\eta)$; but quite the opposite is true with $G(\eta)$. It is noticed that the effect of increasing values of β is to reduce the thickness of the fluid velocity in the boundary layer and increase the dust-phase transverse velocity, as well as the horizontal velocity.

Figs 2(a) - 2(d) exhibit the transverse velocity $f(\eta)$, the horizontal velocity $f'(\eta)$, the particle transverse velocity $F(\eta)$ and the particle horizontal velocity $G(\eta)$ profiles for several sets of values of K_1 and β_1. The effect of porous parameter on the velocity of fluid elements above the sheet appears to become less pronounced for the Maxwellian fluid, i.e., by an increase in the elasticity level of the fluid. A larger velocity

adjacent to the surface means lower velocity gradient with a subsequent drop in the surface shear stress and thereby the force required to drag the sheet. It is evident from the Figs. 2(a)- 2(d) that the effect of increasing values of Maxwell parameter is to reduce the fluid velocity in the boundary layer and the dust-phase horizontal velocity, but quite opposite is found in dust-phase transverse velocity.

Figures 3 - 5 shows the fluid temperature $\theta(\eta)$ and dust-phase temperature $\theta_p(\eta)$ profiles for the different values of the governing parameters. The general trend is that the fluid-temperature distribution is unity at the surface , whereas the dust-phase temperature is not. However, with the changes in the governing parameters both asymptotically tend to zero as the distance increases from the boundary. Figs 3(a) and 3(b) illustrates the effect of K_1 and β on $\theta(\eta)$. The effect of increasing values of K_1 is to increase $\theta(\eta)$ and also $\theta_p(\eta)$. From the graphical representation, the porous parameter has a significant effect on the temperature profiles above the sheet. As K_1 increases there is an increase in the temperature profile as well as the dust-phase profile. The effect of β is to decrease the temperature profile that in turn reduces the thickness of the thermal boundary, whereas it enhances the dust-phase temperature at the surface and, hence, increases the thickness of the dust-phase temperature. Figs 4(a) and 4(b) exhibit the fluid-temperature distribution and dust-phase temperature distribution for several sets of values of the K_1 and β_1. The effect of the porous parameter on the temperature profiles becomes less significant for Maxwell fluids, i.e., for elastic liquids. The effect of β_1 is to increase the fluid temperature and the dust-phase temperature. This is due to the fact that the thickening of the thermal boundary layer occurs due to an increase in the elasticity stress parameter, however, the temperature distribution asymptotically tends to zero as the distance increases from the boundary. The graphs for $\theta(\eta)$ and $\theta_p(\eta)$ for different values of the ε *and* Pr are, respectively, shown in Figs. 5(a) and 5(b). These figures demonstrate that an increase in ε results in an increase the temperature profile $\theta(\eta)$ as well as $\theta_p(\eta)$. This is due to the fact that the assumption of temperature-dependent thermal conductivity (linear form) implies a reduction in the magnitude of the transverse velocity by a quantity $\partial K(T)/\partial y$ as can be seen from the heat transfer equation. Also, we observe that the effect of Pr is to decrease both $\theta(\eta)$ as well as $\theta_p(\eta)$. Finally, the effects of all the physical parameters on the surface-velocity gradient, the particle-velocity components, particle-density component, the temperature gradient, and the dust-phase temperature, respectively, at the sheet are depicted in Table 2. It is of interest to note that the effect β_1, K_1 *and* β is to increase the magnitude of the skin friction coefficient. The effect of $\varepsilon, \beta_1,$ *and* K_1 is to decrease the magnitude of the temperature gradient at the sheet, whereas the reverse trend is observed with an increase in Pr *and* β. From Table 2, it is further noticed that the effect of K_1 *and* β is to increase the dust-phase temperature as well as the particle velocity component. This observation is true for zero and nonzero values of K_1.

5. Conclusion

Some of the interesting observations are:

- The effect of increasing values of the fluid-particle interaction parameter, Maxwell parameter and the porous parameter is to decrease the velocity throughout the boundary layer.
- The effect of increasing values of the fluid-particle interaction parameter is to reduce the fluid temperature. However, quite opposite is found in particle phase temperature.
- The effect of Maxwell parameter, porous parameter and variable thermal conductivity parameter is to enhance the fluid temperature as well as the particle phase temperature in the flow region.
- The thermal boundary layers of the fluid and the dust phase are highly influenced by the Prandtl number. The effect of Pr is to decrease the thermal boundary layer thickness.

References

1. B.C. Sakiadis, Boundary-layer behavior on continuous solid surfaces I, The boundary layer on a equations for two dimensional and axisymmetric flow, A.I.Ch.E.J., 7 (1961) 26-28.
2. L.J. Crane, Flow past a stretching plate, ZAMP, 1 (1970) 645-647.
3. L.G. Grubka, K.M. Bobba, Heat transfer characteristics of a continuous stretching surface with variable temperature, ASME J. Heat Transf. 107 (1985) 248–250.
4. B.K. Dutta, P. Roy, A.S. Gupta, Temperature field in flow over a stretching sheet with uniform heat flux, Int.Comm.Heat Mass Transf., 12 (1985) 89-94.
5. C.K. Chen, M.I. Char, Heat transfer of a continuous stretching surface with suction or blowing, J. Math. Anal. Appl., 135 (1988) 568-580.
6. M.E. Ali, Heat transfer characteristics of a continuous stretching surface, Heat Mass Transf., 29 (1994) 227–234.
7. A. Ishak, R. Nazar, I. Pop, Boundary layer flow and heat transfer over an unsteady stretching vertical surface, Meccanica, 44 (2009) 369–375.
8. Prasad, K.V., Vajravelu, K, Vaidya, H , MHD Casson Nanofluid Flow and Heat Transfer at a Stretching Sheet with Variable Thickness, Journal of Nanofluids, Vol.5, (3), 2016, pp. 423-435(13).
9. Prasad, K. V.; Vajravelu, K.; Shivakumara, I. S.; Vaidya, Hanumesh; Basha, Neelufer. Z., Flow and Heat Transfer of a Casson Nanofluid Over a Nonlinear Stretching Sheet, Journal of Nanofluids, Vol.5, 2016, pp. 743-752(10).
10. K. V. Prasad, Hanumesh Vaidya, K. Vajravelu, and V. Ramanjini , Analytical Study of Cattaneo-Christov Heat Flux Model for Williamson-Nanofluid Flow Over a Slender Elastic Sheet with Variable Thickness , J. Nanofluids (2018) 7, 583–594.
11. K.V. Prasad, K. Vajravelu, Hanumesh Vaidya, B. T. Raju, Heat Transfer in a Non-Newtonian Nanofluid Film Over a Stretching Surface. Journal of Nanofluid 4 (2015) 1-12.
12. K. V. Prasad, K. Vajravelu, Hanumesh Vaidya, M. M. Rashidi, and Neelufer .Z.Basha ,Flow and Heat Transfer of a Casson Liquid over a Vertical Stretching Surface: Optimal Solution , American Journal of Heat and Mass Transfer (2018) Vol. 5 No. 1 pp. 1-22 doi:10.7726/ajhmt.2018.1001.
13. K.R. Rajagopal, T.Y. Na, A.S. Gupta, Flow of a visco-elastic fluid over a stretching sheet, Rheol. Acta., 23 (1984) 213-215.
14. R.K. Bhatnagar, G. Gupta, K.R. Rajagopal, Flow of an Oldroyd-B fluid due to a stretching sheet in the presence of a free stream velocity, Int. J. Non-Linear Mech., 30 (1995) 391-405.
15. K. Sadeghy, A.H. Najafi, M.Saffaripour,(2005) Sakiadis flow of an upper-convected Maxwell fluid. Int J Non-Linear Mech 40 (2005) 1220–1228
16. K. Vajravelu, K.V. Prasad, A. Sujatha, Convection heat transfer in a Maxwell fluid at a non-isothermal surface, Cent. Eur. J. Phys., 9 (2011) 807-815.
17. P.G. Saffman, On the stability of laminar flow of a dusty gas, J. Fluid. Mech., 13 (1962) 120-128.
18. N. Datta, S.K. Mishra, Boundary layer flow of a dusty fluid over a semi-infinite flat plate, Acta Mech., 42 (1982) 71-83.
19. Xie Ming-Liang, Lin Jian-Zhong, Xing Fu-Tang, On the hydrodynamic stability of a particle-laden flow in growing flat plate boundary layer, J. Zhejiang Uni. SCI. A, 8 (2007) 275-284.
20. K. Vajravelu and K.V. Prasad, Keller-box method and its application (HEP and Walter De Gruyter GmbH, Berlin/Boston, 2014).

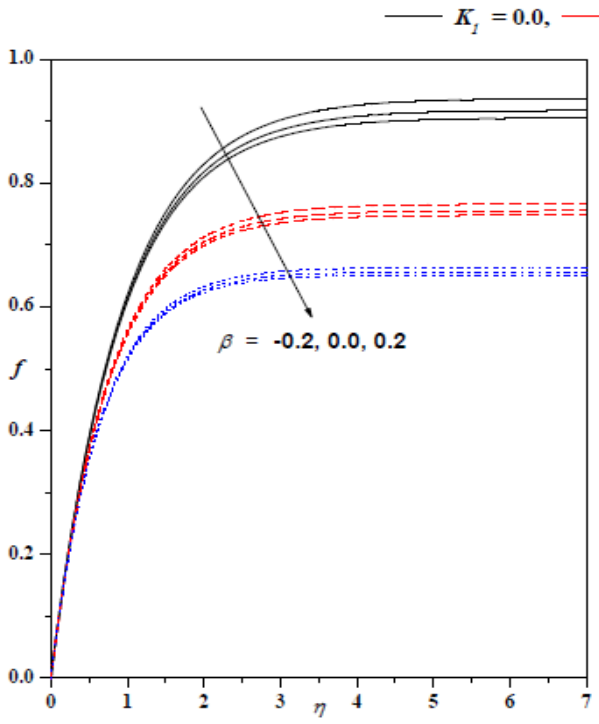

Fig. 1(a): Transverse velocity profiles for different values of β and K_1

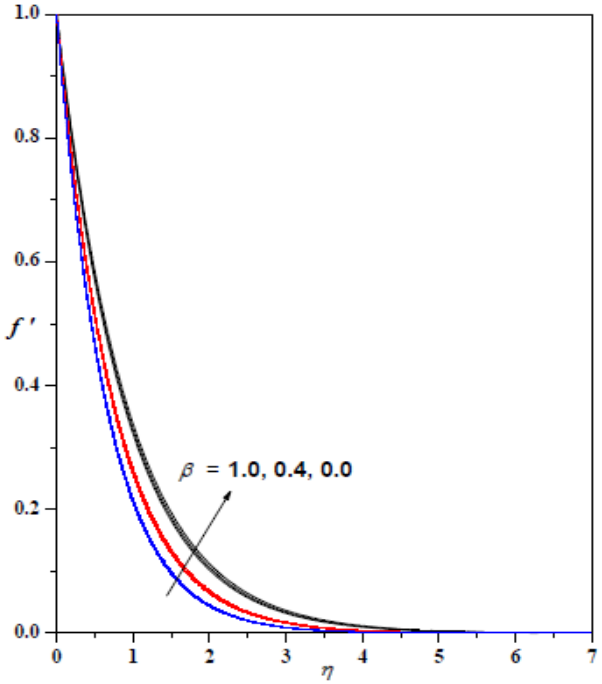

Fig. 1(b): Horizontal velocity profiles for different values of β and K_1

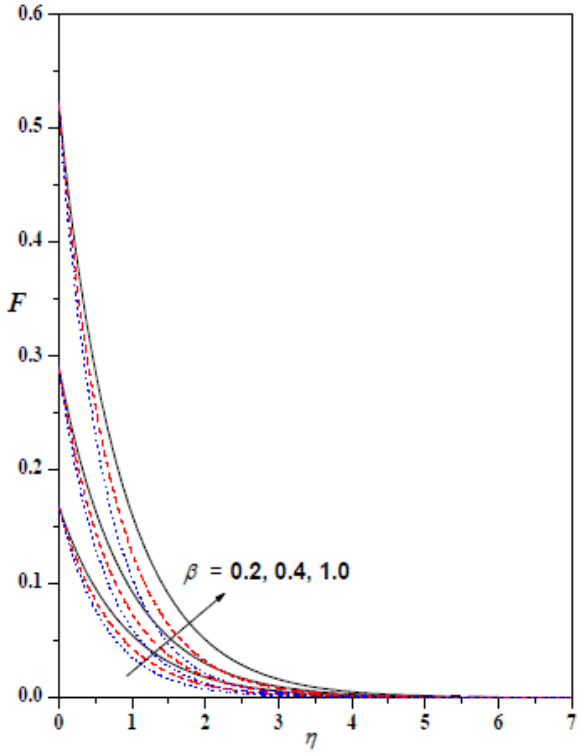

Fig. 1(c): Particle velocity components F for different values of β and K_1

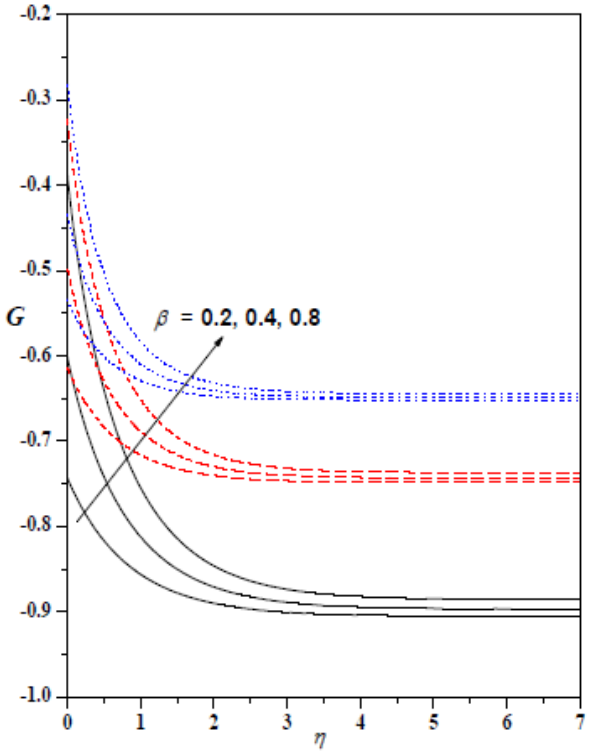

Fig. 1d): Particle velocity components G for different values of β and K_1

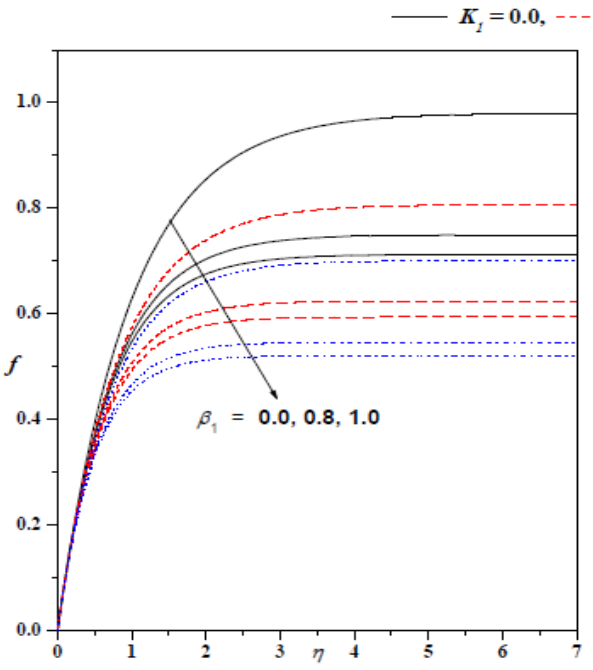

Fig. 2(a): Transverse velocity profiles for different values of β_1 and K_1

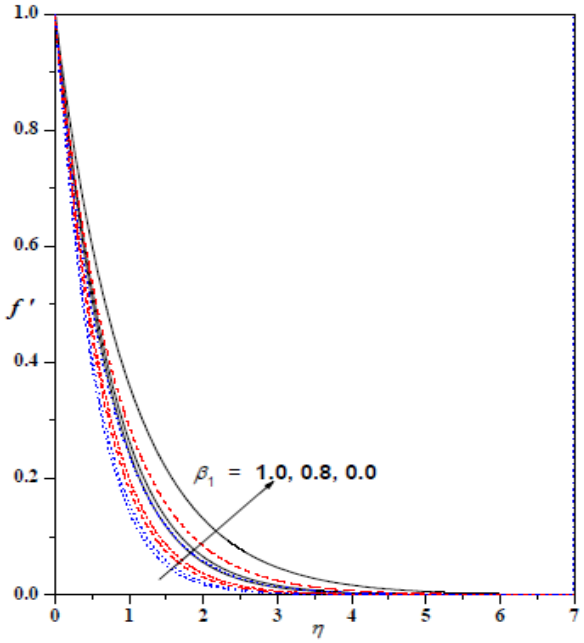

Fig. 2(b): Horizontal velocity profiles for different values of β_1 and K_1

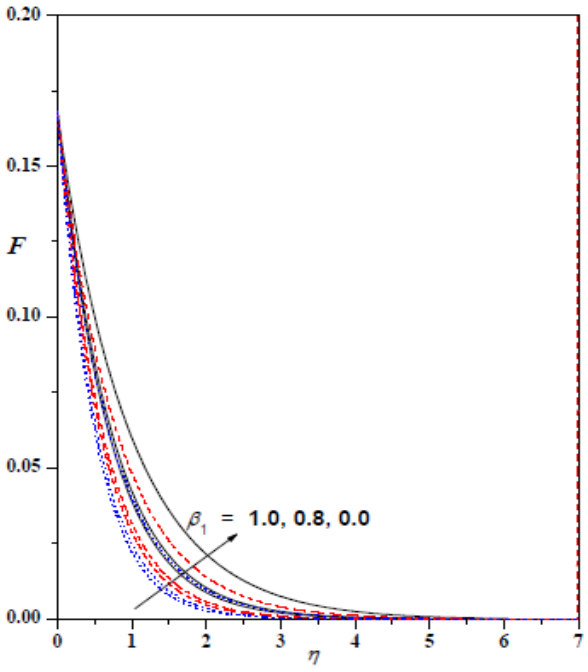

Fig. 2(c): Particle velocity components F for different values of β_1 and K_1

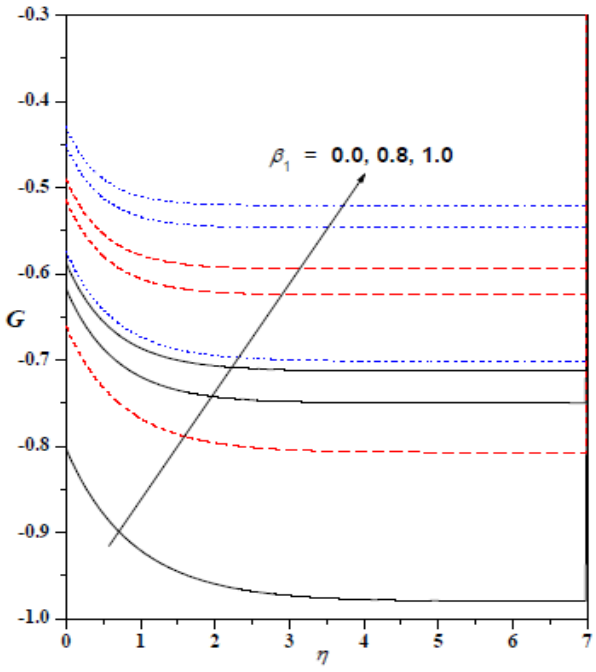

Fig. 2(d): Particle velocity components G for different values of β_1 and K_1.

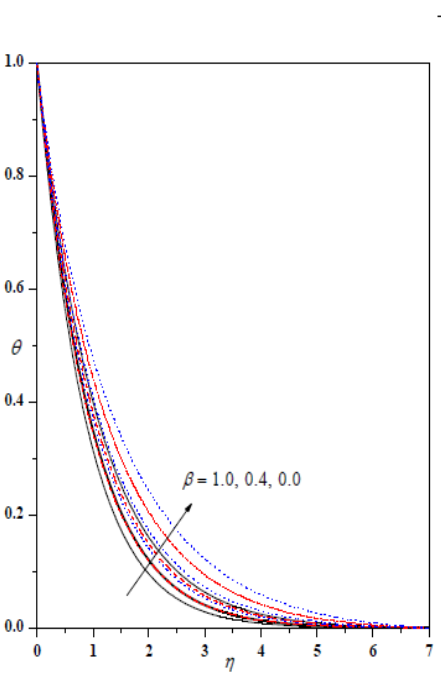

Fig. 3(a): Fluid temperature profiles for different values of β and K_1

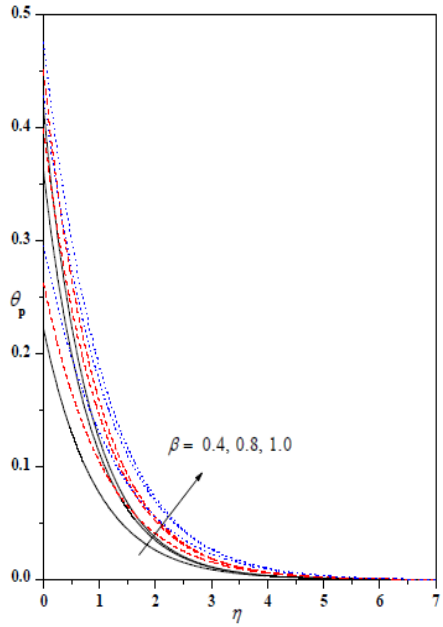

Fig. 3(b): Dust-phase temperature profiles for different values of β and K_1

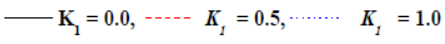

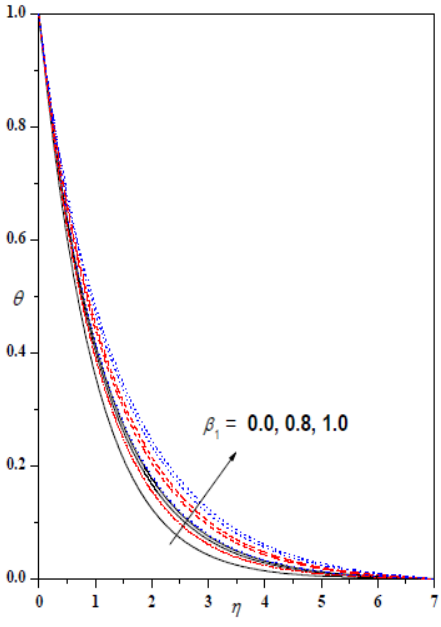

Fig. 4a): Fluid temperature profiles for different values of β_1 and K_1

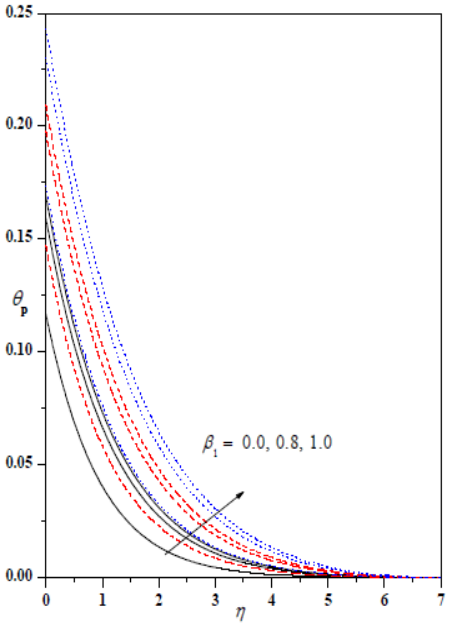

Fig. 4(b):Dust-phase temperature profiles for different values of β_1 and K_1

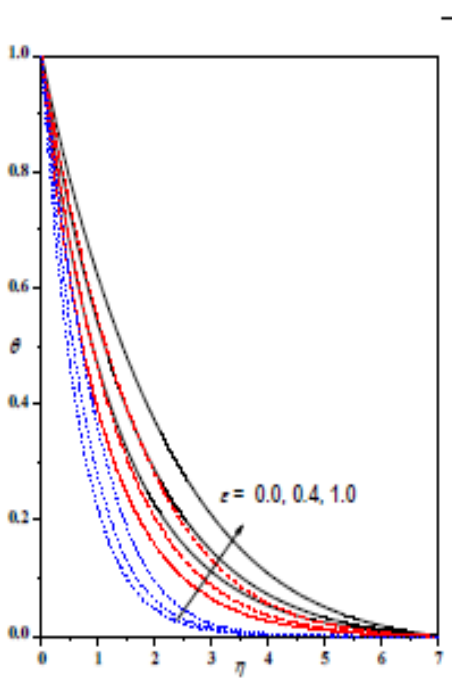

Fig. 5(a): Fluid temperature profiles for different values of ε and *Pr*

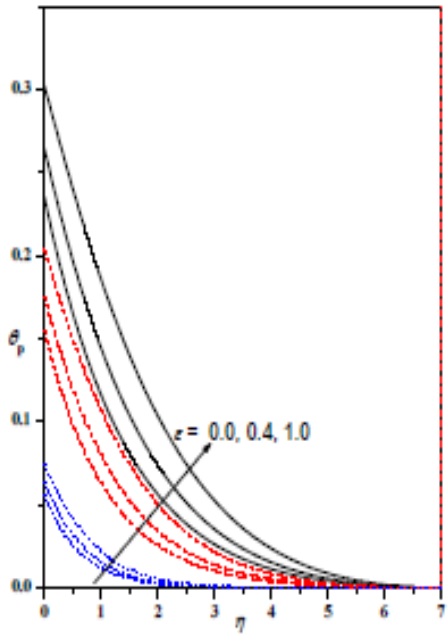

Fig. 5(b): Dust-phase temperature profiles for different values of ε and *Pr*

Table 1. Comparison of some of the values of $-\theta'(0)$ when $\beta = 0.0$, $K_1 = 0.0$ and $\varepsilon = 0.0$.

When $\beta_1 = 0.0$	Pr = **0.72**	Pr = **1.0**	Pr = **3.0**	Pr = **6.7**	Pr = **10.0**
Grubkha and Bobba [3]	0.8086	1.0000	1.9237	-	3.7207
Ali [6]	0.8058	0.9961	1.9144	-	3.7006
Ishak et al. [7]	0.8086	1.0000	1.9237	3.0003	3.7207
Present results	0.808836	1.000000	1.923687	3.000272	3.720788
When $\Pr = 1.0$	β_1 = **0.0**	β_1 = **0.2**	β_1 = **0.4**	β_1 = **0.6**	β_1 = **0.8**
Vajravelu et al.[16]	1.0001743	0.9800923	0.9607879	0.9423181	0.9246983
Present results	1.000174	0.9800925	0.9607877	0.9423183	0.9246984

Table.2: **Numerical values of skin friction $f''(0)$, the particle velocity components $F(0), G(0)$, the particle density component $H(0)$, the wall temperature gradient $\theta(0)$, and the wall temperature dust particles $\theta_p(0)$ for different values of the physical parameters.**

Pr	ε	β_1	K_1	β	$f''(0)$	$F(0)$	$G(0)$	$H(0)$	$\theta'(0)$	$\theta_P(0)$
1.0	0.1	0.2	0.0	0.0	-1.05198	0.00000	-0.91721	0.20000	-0.91331	0.00000
				0.2	-1.06772	0.16766	-0.74287	0.20335	-0.97889	0.12794
				1.0	-1.10203	0.52204	-0.30747	0.26545	-1.11558	0.41699
			0.5	0.0	-1.28079	0.00000	-0.75534	0.20000	-0.85530	0.00000
				0.2	-1.29379	0.16766	-0.61388	0.20335	-0.92853	0.16030
				1.0	-1.32234	0.52206	-0.25620	0.26541	-1.06476	0.45086
			1.0	0.0	-1.47454	0.00000	-0.65650	0.20000	0.80837	0.00000
				0.2	-1.48586	0.16766	-0.53473	0.20335	-0.88773	0.18858
				1.0	-1.51082	0.52207	-0.22422	0.26538	-1.02239	0.47543
1.0	0.1	0.0	0.5	0.0	-1.22475	0.00000	-0.81593	0.20000	-0.87683	0.00000
				0.2	-1.23838	0.16746	-0.66061	0.20341	-0.94702	0.14696
				1.0	-1.26830	0.52143	-0.27293	0.26617	-1.08360	0.43885
		0.2	0.5	0.0	-1.28079	0.00000	-0.75534	0.20000	-0.85530	0.00000
				0.2	-1.29379	0.16766	-0.61388	0.20335	-0.92853	0.16030
				1.0	-1.32234	0.52206	-0.25620	0.26541	-1.06476	0.45086
		1.0	0.5	0.0	-1.48979	0.00000	-0.59761	0.20000	-0.77975	0.00000
				0.2	-1.50079	0.16813	-049030	0.20319	-0.86330	0.20926
				1.0	-1.52507	0.52368	-0.20987	0.26349	-0.99637	0.48877
1.0	0.0	0.2	0.5	0.0	-1.28083	0.00000	-0.75394	0.20000	-0.92319	0.00000
				0.2	-1.29379	0.16766	-0.61381	0.20335	-0.99709	0.15460
				1.0	-1.32237	0.52207	-0.25617	0.26537	-1.14308	0.44341
	0.2	0.2	0.5	0.0	-1.28083	0.00000	-0.75394	0.20000	-0.80431	0.00000
				0.2	-1.29379	0.16766	-0.61381	0.20335	-0.87099	0.16510
				1.0	-1.32237	0.52207	-0.25617	0.26537	-1.00004	0.45719
	0.4	0.2	0.5	0.0	-1.28083	0.00000	-0.75394	0.20000	-0.71619	0.00000
				0.2	-1.29379	0.16766	-0.61381	0.20335	-0.77751	0.71511
				1.0	-1.32237	0.52207	-0.25617	0.26537	-0.89403	0.46915
0.72	0.1	0.2	0.2	0.0	-1.22475	0.00000	-0.81593	0.20000	-0.70200	0.00000
				0.2	-1.29379	0.16766	-0.61381	0.20335	-0.76722	0.24194
				1.0	-1.28833	0.70817	-0.06469	0.52063	-0.90682	0.54564
1.0	0.1	0.2	0.2	0.0	-1.22475	0.00000	-0.81593	0.20000	-0.87683	0.00000
				0.2	-1.29379	0.16766	-0.61381	0.20335	-0.92890	0.15991
				1.0	-1.28833	0.70817	-0.06469	0.52063	-1.08360	0.43885
2.0	0.1	0.2	0.2	0.0	-1.22475	0.00000	-0.81593	0.20000	-1.36681	0.00000
				0.2	-1.29379	0.16766	-0.61381	0.20335	-1.39216	0.05796
				1.0	-1.28833	0.70817	-0.06469	0.52063	-1.54268	0.23531
5.0	0.1	0.2	0.2	0.0	-1.22475	0.00000	-0.81593	0.20000	-2.33917	0.00000
				0.2	-1.29379	0.16766	-0.61381	0.20335	-2.34460	0.01386
				1.0	-1.28833	0.70817	-0.06469	0.52063	-2.45253	0.08022
10.0	0.1	0.2	0.2	0.0	-1.22475	0.00000	-0.81593	0.20000	-3.43155	0.00000
				0.2	-1.29379	0.16766	-0.61381	0.20335	-3.42930	0.00473
				1.0	-1.28833	0.70817	-0.06469	0.52063	-3.50713	0.03229